STRUCTURAL CONTROL AND HEALTH MONITORING
Struct. Control Health Monit. (2009)
Published online in Wiley InterScience
(www.interscience.wiley.com). DOI: 10.1002/stc.350

Earthquake damage detection in the Imperial County Services Building II: Analysis of novelties via wavelets

Maria I. Todorovska*,†,‡ and Mihailo D. Trifunac§

Department of Civil Engineering, University of Southern California, Los Angeles, CA 90089-2531, U.S.A.

SUMMARY

The former Imperial County Services Building is a rare case of an instrumented building damaged by an earthquake. In this paper, it is used to test a structural health monitoring method, based on detecting novelties in the recorded seismic response, by examining the correlation between their occurrence, spatial distribution and magnitude with the degree of the observed damage. The novelties are detected using expansion in a basis of bi-orthogonal wavelets. For this building, most of the larger novelties can be associated with the observed damage. The novelties suggest that damage first occurred at about 6.4 s, proceeded between 8.2 and 9.2 s, and culminated at about 11.2 s with the collapse of the first story columns at the east end of the building. These times are consistent with large inter-story drifts, and significant drops in the NS and EW system frequencies, reported previously. The major damage followed large pulses of input power within about 2 s. The time delays between novelties in different recording channels indicate velocity of propagation of the disturbances within the structure, consistent with other independent estimates. Copyright © 2009 John Wiley & Sons, Ltd.

KEY WORDS: damage detection; structural health monitoring; wavelets; novelties detection; earthquake response; vibration; wave propagation in structures; Imperial County Services Building

INTRODUCTION

The former Imperial County Services (ICS) Building was a six-story reinforced concrete structure in El Centro, California, which was severely damaged by the Imperial Valley earthquake of October 15, 1979 ($M_L = 6.6$, depth $H = 8$ km), and later demolished [1]. The closest distance from the rupture was ~ 7 km [2]. This building was instrumented by a 13 channel central recording system (CR-1) and a free-field site, which all recorded the earthquake.

*Correspondence to: Maria I. Todorovska, Department of Civil Engineering, University of Southern California, Los Angeles, CA 90089-2531, U.S.A.
†E-mail: mtodorov@usc.edu
‡Research Professor.
§Professor.

Received 7 August 2008
Revised 3 May 2009
Accepted 12 June 2009

This building is a rare case of an instrumented building damaged by an earthquake, and provides an opportunity to explore, develop, test and validate different structural health monitoring methods, in the realistic *full-scale* environment and for *actual earthquake response* data. This paper is part of a sequence of papers on examining different structural health monitoring methods by comparison of their assessments, based on the recorded data, with the observed damage in this building, and by checking the consistency of the results by different methods. In the first paper of the sequence [3], we performed the most elementary analyses of detecting drops in the building 'instantaneous' frequencies of vibration, and increases in the inter-story drifts [4,5]. The building frequencies were determined by time–frequency analysis using Gabor transform, and are those of the soil–structure system [6], which depend on the properties of the soil and foundation system. The computed inter-story drifts also include the contribution from rigid body rocking of the building. Consequently, the detected drops in the frequency of vibration and large inter-story drifts were not necessarily only due to damage. In another paper [7], we tested a new method based on detecting changes in wave travel time through this building, which depends only on the properties of the structure.

This paper examines a damage detection method based on detecting abrupt changes ('novelties' or 'surprises' in the jargon of data mining) in the recorded seismic response. This method is based on the assumption that sudden loss of stiffness due to a localized damage would cause (directly or indirectly) abrupt changes in the response that would produce novelties with magnitude proportional to the degree of damage and the closeness of the sensor to the location of the damage. The novelties are detected by expanding the motion in the high–frequency band 12.5–25 Hz in series of bi-orthogonal wavelets, and analysis of spikes in the plots of the square wavelet coefficients versus the central time of the corresponding wavelet. Applications to numerically simulated response of simple models with postulated damage [8–14] have shown that this method *can point out the time of damage*, but the changes are detectable only if the spikes in the wavelet coefficients are above the noise. Also, the detected changes are more prominent if the sensor is closer to the location of the damaged member, and *may be difficult to detect if the sensor is far from the damage*. Hence, this method requires a relatively dense array of sensors, and its spatial resolution depends on the configuration and inter-sensor spacing. The method of novelties has also been tested experimentally on a laboratory structure representing a simplified model of a metallic aircraft wing box, Gnat aircraft and aircraft wing [15–17]. There have been very few related applications to earthquake response data in buildings [12,18], which have demonstrated the *existence* of novelties in earthquake records in damaged buildings, but no clear correspondence to the observed damage. To the knowledge of the authors, the analysis of the ICS building, presented in this paper, is the first in depth analysis of the method applied to actual earthquake response data recorded in structures. Results of earlier stages of this analysis were reported in [19,20], which describe the correspondence between the spatial distribution and amplitudes of the detected novelties and the observed damage, and a preliminary analysis of the 'noise' in this method (i.e. novelties not caused by significant damage), and of travel times of high–frequency disturbances in the structure.

The objective of this paper is to examine whether this method can detect the location and degree of damage in real structures, in the presence of *realistic noise*, which is not stationary white noise, as is usually assumed in numerical simulations. Following a brief review of the methodology, the spatial occurrence of novelties throughout the structure and their magnitude are compared against the observed damage after the earthquake [1], which represents the cumulative damage at the end of shaking, but contains no information about how the damage

DOI: 10.1002/stc

evolved in time. Coincidence of novelties with large inter-story drifts is used as independent information in unfolding the occurrence of damage in time, and in verifying if the novelty could be associated with damage. This is followed by an analysis of time delays between a group of novelties assumed to have a common causative event (occurrence of damage, or a pulse from the input ground motion), and the spatial distribution of their amplitudes. The time delays and distances between sensors are used to estimate the velocity of propagation of the disturbances throughout the structure, and these estimates are compared against the average shear wave velocity of vertically propagating waves estimated from the first system frequency [3], representing a lower bound. Further, the time of occurrence of the major damage, deducted from the analysis of novelties, is compared against the time history of variations of the NS and EW system frequencies as another independent indicator of damage [3], and against the time history of the power and energy of the input ground motion. The final section describes the conclusions about the effectiveness of the method and the insight gained.

In structural health monitoring literature, which largely deals with numerically simulated case studies, damage is detected by comparison of patterns seen in data from the damaged state against those seen in data from the undamaged state. For this building, no earthquake data are available from the undamaged state to compare patterns in the data, but description of *observed physical damage* is available, and 'damage' refers to an observation as reported in [1]. Distinguishing between novelties caused by different type of damage is out of the scope of this paper. The damage in this building was severe and obvious, while the challenge is to detect reliably smaller and hidden damage. Vibrational data recorded in full-scale damaged buildings during the causative event, however, are rare, and there are clear advantages of using such data to test methods even if the damage was severe and obvious. As pointed out in [3], analysis of such data can provide valuable information about the capabilities of a method and its sensitivity to *noise in real data*, beyond what can be learned from analysis of numerically simulated data. Some obvious advantages are as follows. The earthquake response data recorded in damaged full-scale structures involve realistic materials, boundary conditions and excitation, each contributing to the realistic noise in the related estimation process. Comparison of the detected changes in the monitored parameters due to severe damage with realistic noise can help assess the limits of a method to detect less severe damage. Further, the capabilities of different methods in a real environment can be compared, which can help select directions for future research. Finally, in this study we use discrete wavelet transform as one possible method to detect novelties, and we discuss implications of using different wavelets. Comparison of this method with other methods for novelty detection is out of the scope of this paper.

METHODOLOGY

Detection of novelties using wavelets

Abrupt changes in a signal, or novelties, can be detected by passing the data through some running difference filter. A way to do such filtering, within the framework of multiresolution analysis, is to use an expansion of the signal in a wavelet basis. Multiresolution analysis was proposed by Mallat [21], who saw the connection between sub-band decomposition and wavelet basis decomposition of a signal. It represents a framework for the construction of wavelet bases. It consists of splitting a signal $f(t)$ into higher and lower frequency components, $D_1(t)$ and $A_1(t)$, by application of high-pass and low-pass filters $H_1(\omega)$ and $H_2(\omega)$, and recursively repeating this

DOI: 10.1002/stc

to the output of the low-frequency filter. After J steps, the signal is decomposed into J high-frequency components, $D_j(t), j = 1, \ldots, J$ and the low-frequency component of the last step of filtering, $A_J(t)$. At each step, the low-frequency component represents a lower resolution *smooth approximation* of the signal, and the high-frequency component represents the higher resolution *detail* that has been removed to create the lower resolution approximation. The resolution of the detail decreases progressively with the increasing level of decomposition. At each level, the smooth approximation reveals the *trends*, and the detail component reveals the *novelties* (surprises) in the data at the particular resolution level.

To identify the occurrence of damage, the novelties in the highest resolution detail sub-band $D_1(t)$ are analyzed, although an abrupt change in the response (e.g. idealized by a Dirac delta or a Heaviside step function) is broad band and would affect all the sub-bands. This choice is due to the highest possible time resolution of the detection, and the best signal-to-noise ratio for this sub-band. The former follows from multiresolution analysis, and the latter is true because the noise in the detection is the structural response itself, which usually tends to be smaller at higher frequencies. Hence, level 1 decomposition of the signal is sufficient

$$f(t) = A_1(t) + D_1(t) \tag{1}$$

Further, $D_1(t)$ is expanded using a basis of wavelet functions, the existence of which is guaranteed by the multiresolution analysis. Then

$$D_1(t) = \sum_{k \in \mathbb{Z}} d_{1,k} \psi_{1,k}(t) \tag{2}$$

where $\{\psi_{1,k}(t)\}_{k \in \mathbb{Z}}$ are the level 1 wavelets in the basis, which are shifts in time of one another. The coefficients of expansion $d_{1,k}$ are the orthogonal projections of the signal onto the dual basis $\{\tilde{\psi}_{m,n}\}_{m,n \in \mathbb{Z}}$

$$d_{1,k} = \langle \tilde{\psi}_{1,k}, f \rangle \tag{3}$$

where

$$\langle \psi_{m,n}, \tilde{\psi}_{m',n'} \rangle = \begin{cases} 1 & m = m' \text{ and } n = n' \\ 0 & \text{otherwise} \end{cases} \tag{4}$$

For an orthogonal basis $\psi_{m,n} = \tilde{\psi}_{m,n}$. For a discretely sampled signal $f[n]$, $n = 1, ..., N$, a basis of compactly supported wavelets can be used, the coefficients of expansion of which can be efficiently computed by the pyramid algorithm (also called fast wavelet transform), which is asymptotically faster even than the FFT [22]. This would result in detail coefficients $d_{1,k}$, $k = 1, \ldots, N/2$. Abrupt changes would result in larger local values of these coefficients.

There is a large choice of compactly supported wavelet bases, which differ in length, smoothness, symmetry and orthogonality properties. The previous studies used Haar [9,18], or of Daubechies db4 wavelets [8,13,14], the former being discontinuous but symmetric, and the latter—smoother but nonsymmetric, both of which constitute an orthogonal basis. Wavelets with shorter support have better time resolution, but are less smooth and prone to 'picking up' noise. In choosing the best wavelet basis for our application, we looked for *longer support* and *smoother* compactly supported wavelets that would smooth out spurious high values and noise, emphasizing the more significant novelties, and for *symmetric* wavelets, which are 'linear phase' and would not introduce bias in the estimate of the time of the damage. This leads to a choice of

DOI: 10.1002/stc

a bi-orthogonal wavelet basis, as the orthogonal ones cannot be both smooth and symmetric. Specifically, we chose the bior6.8 wavelet basis [23], which has 18-point long impulse response, and is nearly orthogonal, with $\langle \psi_{m,n}, \tilde{\psi}_{m,n} \rangle \approx 0.05$. Figure 1 shows the high-pass wavelet filter impulse response of (top), and the analysis wavelet (bottom) with time scale corresponding to sampling interval $\Delta t = 0.02$ s. Because of the near orthogonality, the analysis and synthesis wavelets (i.e. $\tilde{\psi}_{1,k}$ and $\psi_{1,k}$) are almost identical and indistinguishable by bare eye. Another option to consider is to detect novelties in the highest frequency sub-band of wavelet packet decomposition. Such an expansion would lead to a narrower highest frequency sub-band, e.g. 18.75–25 Hz compared with 12.5–25 Hz, and hence less 'noise' in the signal due to high-frequency energy of the ground motion. However, this would be at the expense of reducing the time resolution, and also would reduce the energy of the signal that is to be detected (i.e. the abrupt change).

Interpretation of the detected novelties

We identify the novelties using wavelet transform of acceleration, as spikes in the distribution of $d_{1,k}^2$ versus the central time of the corresponding wavelet, which represents approximately (as the basis is not exactly orthogonal) the power spectrum density versus time of sub-band $D_1(t)$, and also the nodal energy in the corresponding tile of the time–frequency plane [24]. The corresponding tile is $\Delta n = 2$ samples wide in time and $\Delta\Omega = \pi/2$ radians per sample wide in frequency, and is centered at time $n = 2(k + 1/2)$ samples and frequency $\Omega = 3\pi/4$ radians per sample. Considering the relationship $t = (n - 1)\Delta t$, $v = (\frac{1}{2\pi})\frac{\Omega}{\Delta t}$, where t is time in seconds, v is

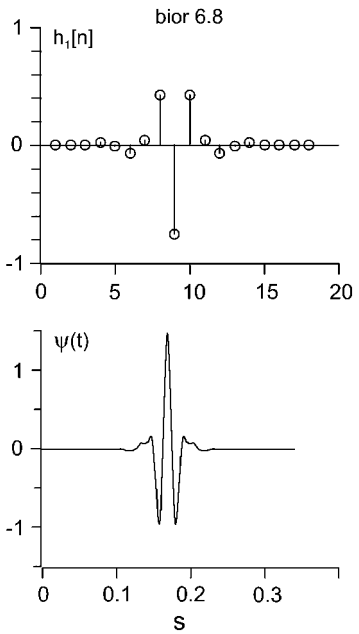

Figure 1. The decomposition high-pass filter coefficients, $h_1[n]$ and the analysis mother wavelet for the bior6.8 wavelet.

DOI: 10.1002/stc

frequency in Hertz and Δt is the sampling interval, and the corresponding tile has dimensions $(2\Delta t\,\mathrm{s}) \times \frac{1}{4\Delta t}\,\mathrm{Hz}$).

We assume a novelty to be a manifestation of a disturbance that was created either within the structure, possibly, but not necessarily, by damage, and *propagated* as wave motion through the structure. A novelty can also be a manifestation of high-frequency pulses of the seismic wave energy from the earthquake source that entered into the building through the base and *propagated* through the structure. During the propagation, these waves are dispersed and attenuated, or amplified by the reflections from the stress free boundaries (e.g. the top and sides) of the building, or due to a concurrent local source. Helpful in the interpretation of the amplitudes of the detected disturbances are the results of numerical simulation of propagation of nonlinear shear waves in a beam using finite differences [25–27]. As the propagation takes finite time, a novelty due to a particular disturbance would appear first in the nearest recording instrument, and with some time delay in the others. The novelties due to the most severe damage are expected to have largest amplitudes and to be seen in most of the recording stations. Those due to a smaller local damage may be seen only locally. A source for a local novelty could also be some other consequence of strong shaking, e.g. impact from falling heavy objects or pounding.

For convenience in tracing the novelties, we name them by using a common name for novelties that appear to be related and are seen in different channels. We call $T_1, T_2, \ldots$ the largest energy novelties that can be seen throughout most of the building, and are likely to be associated with significant damage (here T stands for 'true'). The novelties that can be associated with high-frequency pulses in the ground motion we call $G_1, G_2, \ldots$ if they are seen primarily in the NS response, and $g_1, g_2, g_3, \ldots$ is they are seen mainly in the EW response. Finally, the local novelties, possibly due to smaller local damage or due to some local disturbance other than damage, are marked as $L_1, L_2, \ldots$.

The steps we used in the identification and interpretation of the novelties in our exploratory analysis of the method are as follows: (i) We first identify novelties in the data and classify them. The largest energy novelties that can be associated with the observed damage [1] and are seen in most channels we name $T_1, T_2, \ldots$. The other significant novelties seen locally we name $L_1, L_2, \ldots,$. We also identify the novelties that can be associated with incident waves from the ground motion, and name them appropriately. (ii) Next, we look at the results of damage survey [1] and other dynamic response analyses of this building, identify the locations of the most severe damage and see if those can be associated with the spatial distribution of the novelties in the data. If not clearly identified by large energy novelties, we look further for any patterns in the novelties that might be associated with damage. We compare the timing of the novelties with the timing of changes in the system frequency, and with the occurrence of large drifts. Next, we examine the causality of the novelties, by analysis of travel times, and examine the possibility that some novelties have originated (1) in the input ground motion, or (2) somewhere else in the structure (due to a disturbance caused by 'major' damage), and then propagated to the location of a particular sensor. The causality can be examined and interpreted by measuring the time lags between the novelties.

RESULTS AND ANALYSIS

The ICS Building

The former ICS Building was a six-story reinforced concrete structure in El Centro, California. Here we briefly describe the building, instrumentation layout and the observed damage

DOI: 10.1002/stc

following the Imperial Valley earthquake of October 15, 1979 ($M_L = 6.6$, depth $H = 8$ km), for convenience and completeness of this presentation. Further details about the design, recorded data and observed damage can be found in [1].

Figure 2 shows a photo of a side view of the building, and Figure 3 shows the foundation (top) and a typical floor (bottom) layouts. The ground floor was 41.70 m (136 ft 10 in) by 26.02 m (85 ft 4 in) in plan, and the height of the building was 25.48 m (83 ft 7 in). The foundation consisted of pile caps resting on Raymond-tapered piles, which were interconnected by grade beams (Figure 3 top). Lateral resistance of all levels in the longitudinal (EW) direction was provided by two exterior moment frames along column lines 1 and 4, and two interior moment frames along column lines 2 and 3 (Figure 3). The lateral resistance in the transverse (NS) direction was not continuous. At the ground floor level, it was provided by four short shear walls located along column lines A, C, D and E and extending between column lines 2 and 3 only (Figure 3 top). At the second floor and above, lateral (NS) resistance was provided by two shear walls at the east and west ends of the building (Figure 3 bottom). This caused the building to appear top heavy with a soft first story (Figure 2). The lack of symmetry in the NS stiffness at the ground floor appears to have resulted in excessive torsional response and in significant coupling of the NS and torsional responses. The design strength of the concrete was 34.5 MPa (5 ksi) for the columns, 20.7 MPa (3 ksi) for the elements below ground level, and 27.6 MPa (4 ksi) everywhere else. All reinforcing steel was specified to be grade 40 ($F_y = 276$ MPa).

The building was instrumented by a 13-channel accelerograph array, and a free-field site, which all recorded the earthquake. Figure 4 shows a sketch of the building with the location of the sensors. The film records were digitized by the second author and released as 22.5 s of acceleration data equally sampled at 0.02 s, band-pass filtered with Ormsby filters between 0.1 and 0.125 and 25–27 Hz. The ramp of the low-pass Ormsby filter (25–27 Hz, as chosen in the standard USC accelerogram data processing software package [28]) extends beyond the Nyquist frequency of the time series, to optimize the filter performance, and to make the pass-band amplitudes equal to 1 with accuracy better than 1.2%, between 0 and 25 Hz. In principle, this can introduce minor aliasing errors, between 23 and 25 Hz, but these errors are negligible because the energy in that part of the spectrum is small, and because the spectral amplitudes are reduced by the ramp filter. The ramp filters also reduce the overall error due to the Gibbs

Figure 2. A view (toward North) of Imperial County Services (ICS) building.

DOI: 10.1002/stc

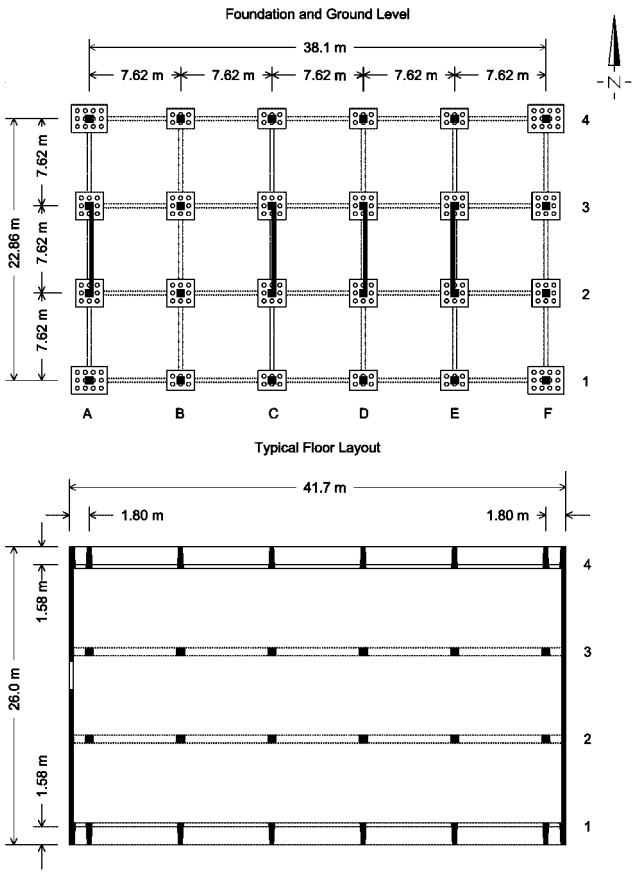

Figure 3. Foundation and ground level plan (top) and typical floor layout (bottom) of the ICS building.

effect [28,29]. The Daubechies filters used in the fast wavelet transform (see Section 'Methodology') are also aliased [22], but are 'perfect reconstruction' filters, the aliasing being cancelled out in the reconstruction.

The recorded peak accelerations at the roof and ground floor were 571 and 339 cm/s^2 in the NS direction and 461 and 331 cm/s^2 in the EW direction. For this analysis, we further high-pass filtered the data at 0.2–0.3 Hz using an Ormsby filter. Figure 5 shows plots of the instrument corrected and band-pass-filtered accelerations.

The building was severely damaged by the earthquake, and was later demolished [1]. Figure 6 shows a schematic representation of the observed damage. The major failure occurred in the columns of frame F (at the east end of the building) at the ground floor. The vertical reinforcement was exposed and buckled, and the core concrete could not be contained, resulting in sudden failure and shortening of the columns subjected to excessive axial loads. This in turn caused an incipient vertical fall of the eastern end of the building, causing cracking of the floor beams and slabs near column line E on the second, third and higher floors. Figure 7(a) shows a photo of the damage of columns F1 and F2 at the ground floor, and Figure 7(b) shows a closer view of the buckled steel bars of column F1. Columns in lines A, B, D and E also

DOI: 10.1002/stc

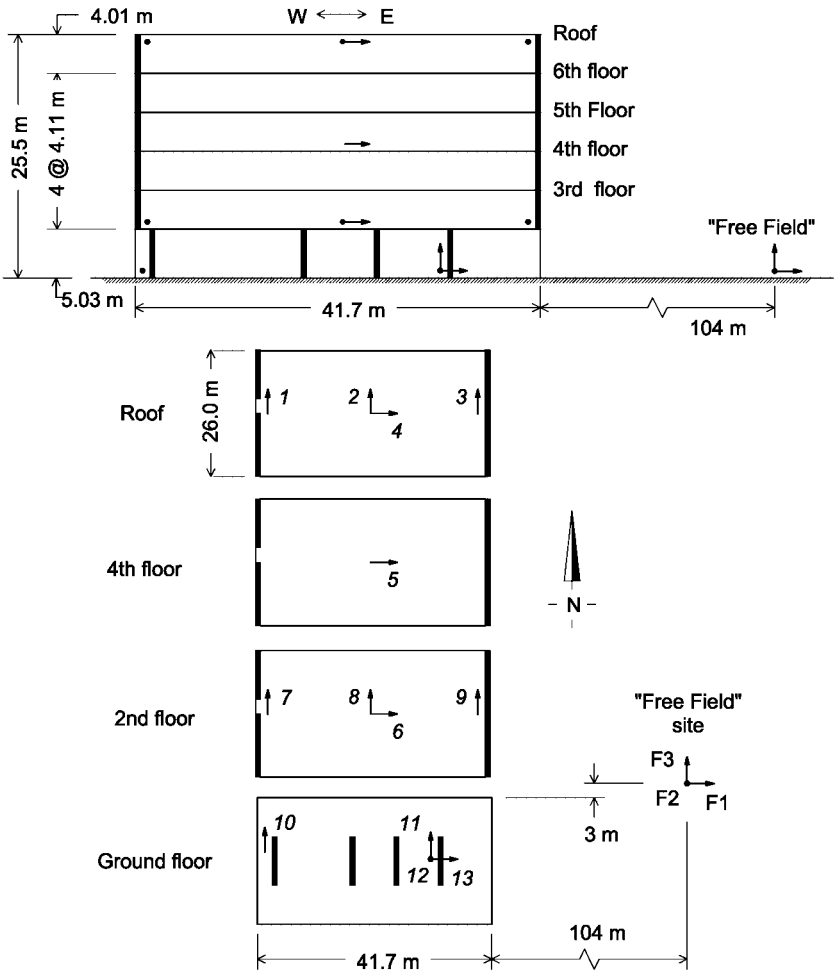

Figure 4. Layout of the seismic monitoring array in the ICS building.

suffered damage. Columns in frames A and E did not suffer as extensive damage as shortening and buckling of the reinforcement in line F at the east side, but large concrete cracks and exposed reinforcement could be seen near the base. In the columns in interior frames B through E, visible cracks and spalling of the concrete cover were also observed [1].

Novelties in the acceleration response

In this section, the novelties are identified in each channel, and correspondence is made between their attributes (location where they are observed and magnitude) and the observed damage. Then, the time of their occurrence is used to make inferences about how the occurrence of damage evolved with time.

The digitized and instrument corrected acceleration data is available sampled at 0.02 s, which corresponds to Nyquist frequency of 25 Hz. Consequently, the level 1 expansion detail sub-band

DOI: 10.1002/stc

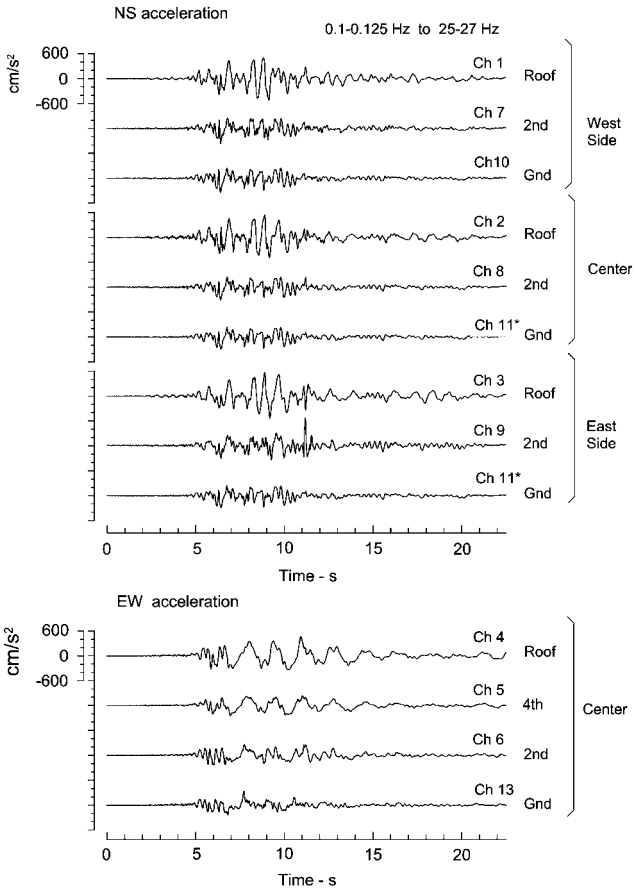

Figure 5. Accelerations (NS and EW components) recorded in the ICS building during the 1979 Imperial Valley earthquake.

spans, for ideal filters, 12.5–25 Hz. For the actual filters used the tapers of the filters extend beyond the ideal range. The squared wavelet coefficients in this sub-band are shown in Figures 8–10, respectively, for the NS motions recorded at the west side, center and east side of the building, and in Figure 11 for the EW motions (recorded only at the center of the building). The novelties for the EW motion are plotted on a different scale, as they are approximately an order of magnitude smaller than those for the NS motions. The drifts (in %) between the corresponding stories are also shown, by a solid line for NS and by a dashed line for EW motions. Novelties T1–T3 (believed to be caused by damage), G1–G3 and g1–g4 (originating in the ground motion, and possibly being magnified by a local occurrence of damage), and L1–L6 (possibly caused by local damage close to the sensor) are identified, and are discussed in the following.

By far the largest novelty is T3, which has amplitude more than an order of magnitude larger than all other novelties (see Figure 10). It occurs in the NS motions at the second floor at the east side of the building (channel 9), which is where the most severe damage (failure of the first story columns of frame F) occurred [1]. It occurs at about 11.2 s after trigger, which is consistent with detected change in the system frequencies attributed to damage [3]. There is also a large

DOI: 10.1002/stc

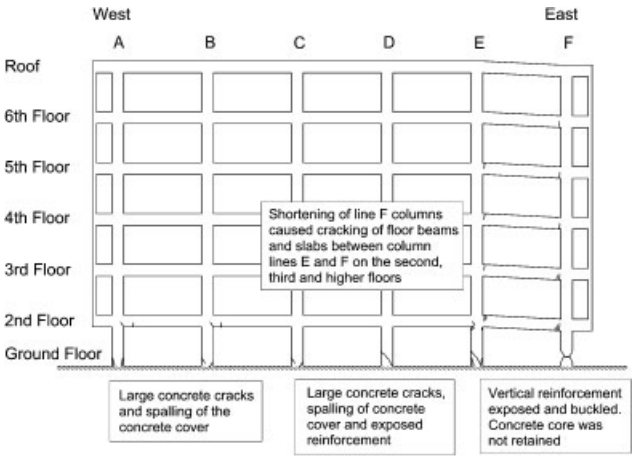

Figure 6. Schematic representation of the damage in the ICS building following the 1979 Imperial Valley earthquake (reproduced from Reference [1]).

Figure 7. (a) Photographs of damage (looking toward south-east): columns F1 and F2 at the ground floor (a), and column F1 (b).

novelty at this time in the NS acceleration at the roof at the east side of the building, also consistent with the spatial distribution of the observed damage. From the plots of drifts in the same figure, it can be seen that at the time of occurrence of T3, the peak EW drift is about 1.5% between the ground and second floors, and about 0.6% between the second floor and the roof. The other two large novelties consistent with the observed damage are T1, which is seen at about 6.3 s after trigger at the second floor at the west side of the building (channel 7), followed by a smaller novelty T2 at about 9.2 s after trigger. Both can be associated with the reported smaller damage on the second floor, at the west side of the building [1].

During the beginning of the recorded motions, novelties originating in the ground motion and propagating vertically through the structure are seen in all the channels, and in both the NS (G1–G3) and the EW motions (g1–g4). In some instances, these are amplified in the structure, possibly by local damage occurring concurrently near the recording stations, caused by large

DOI: 10.1002/stc

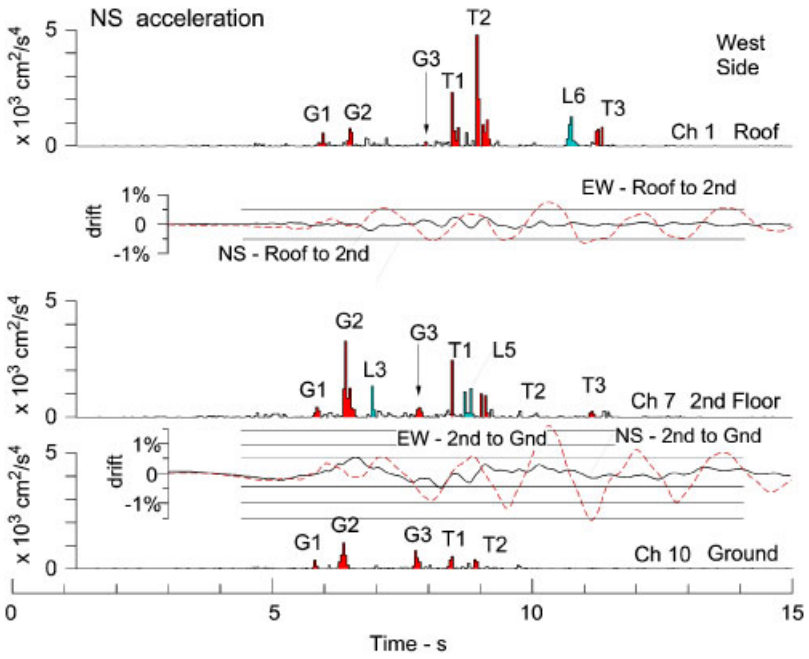

Figure 8. Novelties detected in the NS accelerations at the west end of the building.

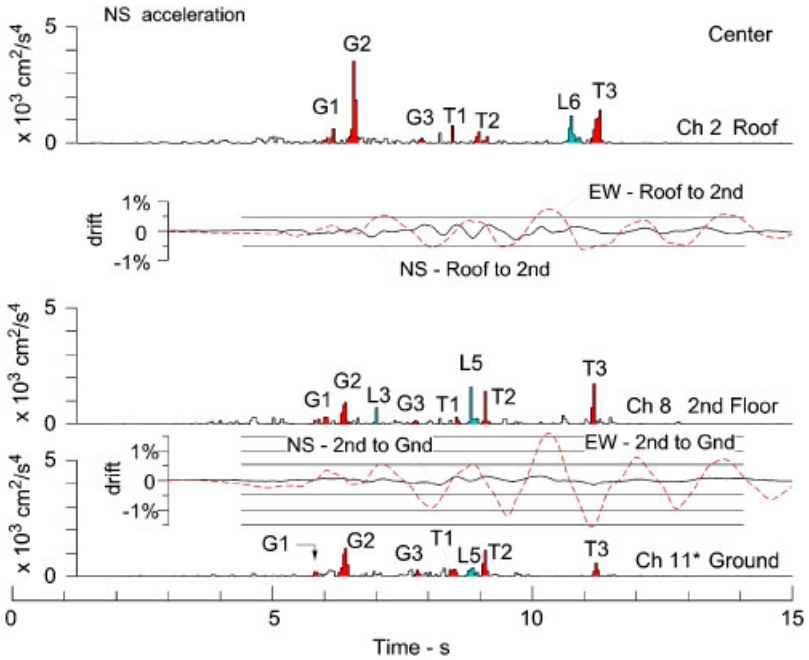

Figure 9. Same as Figure 8 but for the NS accelerations at the center of the building.

DOI: 10.1002/stc

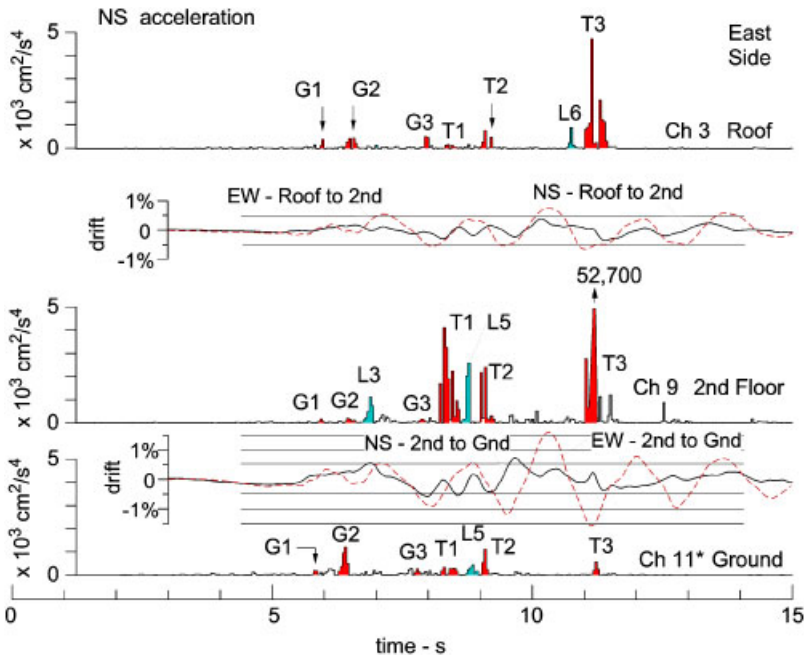

Figure 10. Same as Figure 8 but for the NS accelerations at the east end of the building.

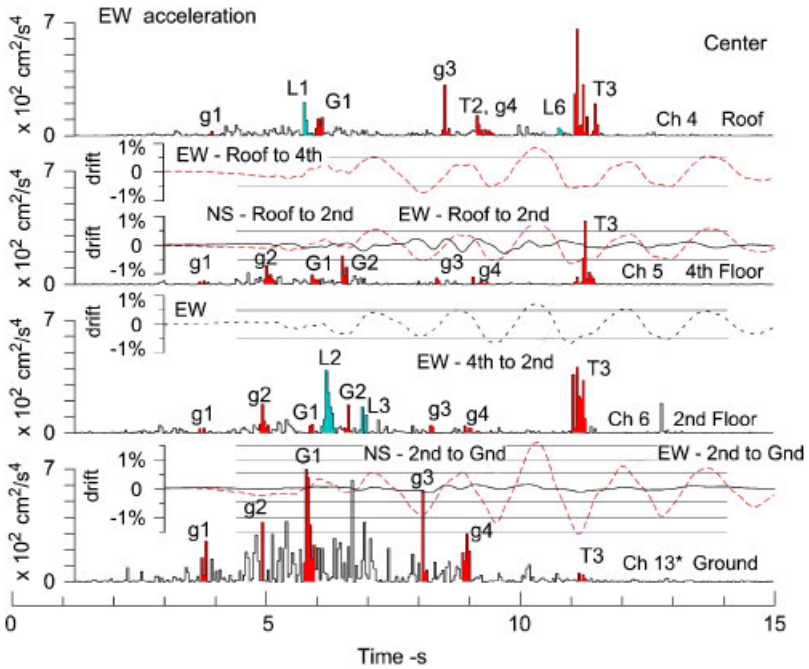

Figure 11. Same as Figure 8 but for the EW accelerations at the center of the building.

DOI: 10.1002/stc

drifts and the passage of wave pulses. That is the case, for example, with G2, which occurs at about 6.3 s, and is seen as amplified in the NS motions at the second floor at the west side of the building (see Figure 8), and also at the roof at the center of the building (see Figure 9).

Next, we consider large novelties in the roof response at the west side of the building seen between 8.5 and 9.5 s (see Figure 8). At this location major damage was not observed. These novelties could be related to local damage very near the sensor, caused by simultaneous large NS and EW drifts, or to T1 and T2. It is also possible that they might have been caused or magnified by some other disturbance than damage that occurred at the roof.

In the EW accelerations, which were recorded only at the center of the building (see Figure 11), prominent novelties are seen at about 11.2 s (T3), on the second and fourth floors, and at the roof, all consistent with the novelties seen in the NS accelerations. Those observed at the second floor and roof are interpreted to be due to the damage identified by novelties T1 and T2 in the NS response, and are named by the same symbols as for the NS response. Novelties are also seen at the second floor, between about 5 and 7 s, interpreted to be due to local damage (L2 and L3) and ground motion pulses G1 and G2. At the roof, novelty L1 appears to be associated with minor local damage.

The analysis of the novelties so far suggests that damage in this building started to occur at the west side of the building at about 6.4 s after trigger of strong motion instruments. The damage at the east side of the building started to occur later, at about 8.3 s after trigger. Additional severe damage occurred between 8.2 and 9.2 s, which further weakened the building, and finally lead to failure of the first story columns at the east side of the building at about 11.2 s, which was felt throughout the building.

Causality and wave travel times

Next, we examine the causality of the novelties detected in different recording channels by measuring the *time lag* between them. One objective of this analysis is to find out if some of the novelties at the roof can be explained by high-frequency pulses in the input motions that have propagated through the building. Another objective is to find out how disturbances, created by the occurrence of damage, propagated through the structure. From the time lags, values of the velocity of shear waves propagating vertically through the building are computed, which are localized in time, and represent average values over the height of the building. To asses if these values are reasonable, they are converted to fixed-base frequency (assuming the building deforms in shear), and compared with the 'instantaneous' soil-structure system frequency estimated by time–frequency analysis [3]. The results of this comparison are shown in Figure 12, for the NS (top) and EW (bottom) components of motion. The thick line shows the 'instantaneous' system frequency v, which represents weighed averages over moving windows in time, and the rectangles in the corners (with area $2\sigma_t \times 2\sigma_v$) indicate the uncertainty of the 'instant' and value of v. These plots also show the times of occurrence of novelties T1, T2 and T3, interpreted to be due to damage. The estimates of fixed-base frequency from the analysis of novelties are shown by open circles, and are explained in the remaining part of this section.

We start the analysis of causality with a small novelty G1 in the NS response seen in both channels 10 and 11 at the ground floor, which occurred at 5.83 s (see Figure 8), before the amplitudes of response became large and before significant damage started to occur. This novelty is apparently due to a pulse in the ground motion, and is seen in the second floor and roof records throughout the building (Figures 8 and 11). At the west side of the building, the

DOI: 10.1002/stc

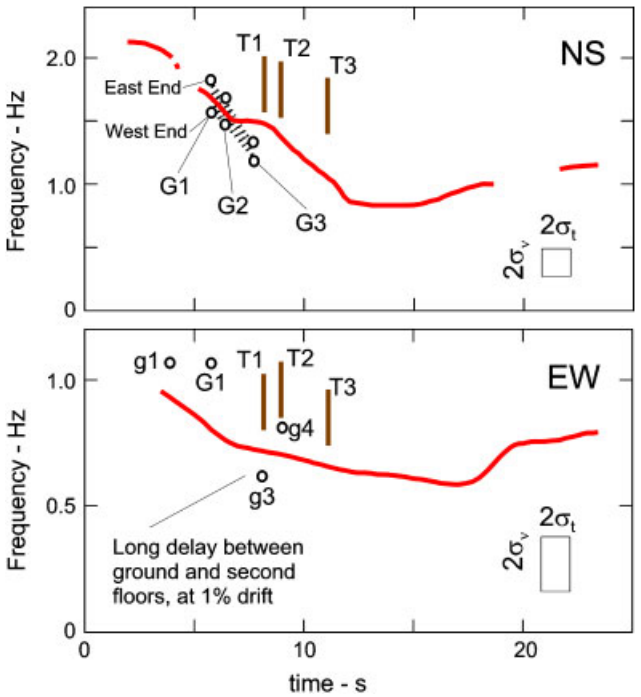

Figure 12. NS (top) and EW (bottom) system frequencies, estimated by time–frequency analysis [3], and times of occurrence of the major damage, estimated from novelties, and frequencies estimated from time lags between novelties.

pulse at the roof is delayed by $\tau = 0.16\,\mathrm{s}$ relative to the ground floor, which implies average velocity of wave propagation in the vertical direction $c_{z,\mathrm{NS}} = H/\tau = 25.5/0.16 = 159\,\mathrm{m/s}$. For a fixed-base model of a building deforming in shear and fixed at the ground floor, assuming that the first mode is a quarter of a wavelength, this wave velocity implies fixed-base frequency $f_{\mathrm{NS,fb}} = c_{z,\mathrm{NS}}/4H = 159/(4 \times 25.5) = 1.56\,\mathrm{Hz}$. At the east side of the building, the time delay is about $\tau = 0.12\,\mathrm{s}$, which implies velocity of propagation $c_{z,\mathrm{NS}} = 202\,\mathrm{m/s}$, and fixed-base frequency 2.03 Hz. These two values for the NS response are not inconsistent with the 'instantaneous' system frequency of 1.6 Hz (from time–frequency analysis [3]) at 5.8 s (Figure 12).

A comparison of the amplitudes of the novelties at the ground floor and at the roof implies that the energy of the pulse at the roof is about 1.5 times the energy of that at the ground floor, which is equivalent to amplitude amplification of 1.2 at the roof. This factor can be explained qualitatively by reduction of amplitude to 0.6 of the amplitude of the input [25], followed by amplification by a factor of 2 due to reflection from the stress-free top of the building.

Next, we analyze the propagation of the pulse identified as G2, which also appears to be due to a high-frequency pulse in the input ground motion. This pulse arrived at the building site at about 6.3 s after trigger, has a larger amplitude than pulse G1, at the west side of the building, and appears to have caused some damage at the west side of the building, near the second floor. Its time coincides with local peaks of the NS and EW drifts between the second and ground floors (respectively of about 0.5 and 0.2%; see Figure 8). This pulse can be traced to the roof

DOI: 10.1002/stc

where it is delayed by $\tau \approx 0.15$ s (at the center and west side of the building; see Figures 8 and 9) to 0.17 s (at the east side of the building; see Figure 10), which also implies vertical shear wave velocity of about $c_{z,\mathrm{NS}} = 150$–170 m/s, and frequency $\nu \approx 1.47$–1.66 Hz (see Figure 12). A comparison of the magnitudes of the novelties implies an overall reduction of the amplitude at the roof by a factor of about 0.8 at the west side and about 0.6 at the east side of the building. A possible explanation for the reduction of amplitude (in contrast to the amplification in the case of G1) is that the damage started to occur concurrently with this pulse [25]. In contrast, the arrival of this pulse at the roof at the center of the building (Figure 10) shows amplification, implying interference with reflected wave from the roof, and possibly some local damage.

Similarly, we follow the propagation of the pulse identified in the NS motions at the ground floor as G3, which occurred at 7.8 s after trigger, and is clearly seen at the west side of the building (Figure 10). The travel time to the roof is about $\tau = 0.19$ s (at the east side of the building; Figure 10) to 0.21 s (at the west side of the building; Figure 8), which implies vertical shear wave velocity $c_{z,\mathrm{NS}} \approx 121$–$134$ m/s, and frequency $\nu \approx 1.19$–1.32 Hz, which is in qualitative agreement with the frequency estimated by time–frequency analysis [3] (Figure 12). The amplitude of the novelties implies reduction of amplitude of the pulse by a factor ~ 0.5. We found only a weak pulse in the center of the building to associate with propagation of G3 (Figure 9).

In contrast to G1, G2 and G3, which we interpret to be due to pulses in the ground motion, delayed at the upper floors, as their energy propagates up into the building, with shear wave velocities of the order of 100 m/s, novelties T1, T2, and T3 exhibit much shorter delays between different floors. We interpret this to be due to compressional crushing and failure of the second story columns, creating high-frequency compressional waves, which propagated through the concrete columns and the shear walls at much higher velocities (of the order of 1–2 km/s in reinforced concrete).

A similar analysis of travel times of ground motion pulses seen only in the EW motion (g1–g4) can also be done, and for the ground motion pulse identified as G1 at about 5.8 s (already considered in NS motions). Pulse G1 reached the roof with a delay of $\tau \approx 0.23$ s, which implies velocity of wave propagation $c_{z,\mathrm{EW}} \approx 111$ m/s, and fixed base frequency $\nu_{\mathrm{EW,fb}} = c_{z,\mathrm{EW}}/4H = 1.09$ Hz. The travel times of pulses g1, g3 and g4, from the ground to the roof were about $\tau \approx 0.23$, 0.41, and 0.31 s, respectively. The corresponding fixed base frequencies are $\nu \approx 1.08$, 0.61 and 0.81 Hz, and the overall average shear wave velocities $c_{z,\mathrm{EW}} \approx 111$, 62 and 82 m/s, respectively. Although the time delays can be measured only approximately, the EW frequencies they imply are not inconsistent with the estimates of 'instantaneous' system frequency [3].

In Reference [7], the estimates of *fixed-base* frequency from novelties were also compared with interval estimates of *fixed-base* frequency obtained from wave travel times measured using impulse response analysis. The former are referred to as 'instantaneous' because of the much smaller window length of the bior6.8 wavelet. As reported in [7], the *instantaneous* estimates are lower than the *interval* estimates, but still higher than the moving window estimates of system frequency, except for pulse g3. Further, the authors state [7] that the lower *instantaneous* estimates from novelties could be explained by the fact that (a) these values are representative of very short time intervals, and hence exhibit larger fluctuations than the smoother *interval* values, which are averages over much longer time windows, and (b) they were typically measured during extreme drift amplitudes (e.g., pulse g3 occurred at a time of about 1% first story drift).

The above analysis suggests that travel times of high-frequency pulses propagating through the building can be measured using wavelet decomposition, and then used to estimate the shear

DOI: 10.1002/stc

wave velocity in the building, which can be done even for complex excitation such as strong ground motion, with further complexities caused by the occurrence of damage. The precision of such an analysis can be improved by using wavelets with a more compact support, and also by using controlled excitation, in post-earthquake testing of damaged structures, in which case it may be possible to detect damage in columns from changes in travel time. Such detailed analyses and refinement of the method are beyond the scope of this study.

Spatial distribution of amplitudes

In the following, we describe the relative amplitudes of four events—G2, T1, T2 and T3—as 'felt' in different channels throughout the building. We do that only for the NS motions, which were recoded by more sensors. Figure 13 shows contours, drawn by hand, of the relative amplitudes of novelties G2, T1, T2 and T3, respectively in (a) through (d).

Event G2 (Figure 13(a)) is the only one in this group that is associated with waves propagating from ground floor up into the building. The novelty associated with this event in channel 7 (on the second floor at the west side of the building) is amplified, likely due to local damage near this sensor, as it coincides with peak drift amplitudes ($\sim$0.5% for NS and $\sim$0.2% for EW motions; Figure 8). The novelty associated with this event in channel 2 (on the roof at the center of the building) is also amplified. The possible causes are the occurrence of some local

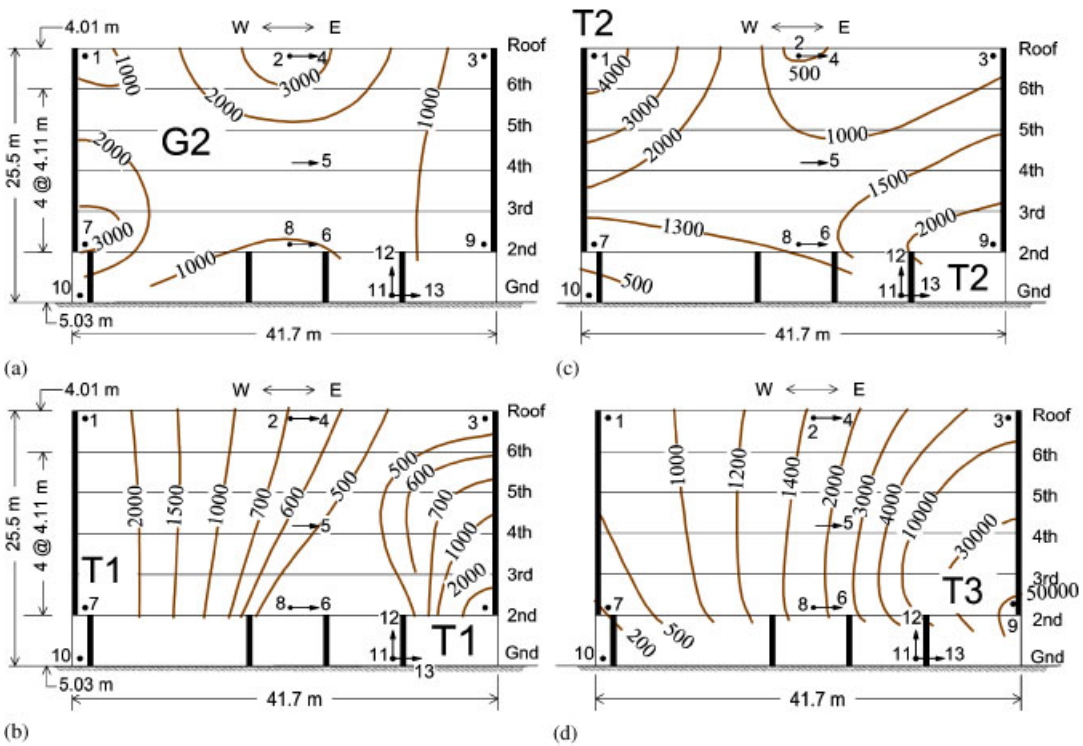

Figure 13. Amplitude of selected novelties (in relative units) felt throughout the building: (a) G2; (b)T1; (c) T2; and (d) T3.

DOI: 10.1002/stc

damage near the sensor at that time, reflection of the pulse from the roof, or some other event near the sensor caused by the strong shaking.

Events T1, T2 and T3 were all associated with significant damage, at the west and east ends of the building. What characterizes those events are large novelties along the end shear walls of the building, which rapidly propagate up and down along these walls, and then spread sideways (west or east) into the building. For event T1 (Figure 13(b)), the novelties are the largest along the west shear wall, with decreasing amplitude toward east, and then have larger amplitudes only in channel 9, on the second floor at the east end of the building. For event T2 (Figure 13(c)), the largest novelty is seen in channel 2 (on the roof at the west end), and near channel 9 (on the second floor at the east end of the building). Finally, at 11.2 s, the columns at the east end of the building (Figure 13(d)) failed, creating the largest novelty in channel 9, which is an order of magnitude larger than all other novelties. The short delay times between the novelties at different stories suggest that the vertical impulse created by the shortening of the columns propagated with a large speed up along the east shear wall, and then toward west, along the floor slabs, with diminishing amplitudes.

Comparison with results of other analyses

Figures 14 and 15, corresponding respectively to the NS and EW response, compare the timing of the novelties indicating the occurrence of major damage (events T1, T2 and T3), with the timing of other indicators of damage. These figures are modified Figures 8 and 9 from [3], which show the results of time–frequency analysis of the roof-relative response. Besides the addition of the timing of novelties T1, T2 and T3 (shown by arrows), the time histories of the first story drifts and the energy and power input into the structure (on a relative scale, as quantities $\mathrm{en}(t)$ and $p(t)$) are also shown. The energy and power of the input motion are proportional to [30]

$$\mathrm{Energy}(t) \sim \mathrm{en}(t) = \int_0^t v^2(\tau)\,\mathrm{d}\tau \tag{5}$$

$$\mathrm{Power}(t) \sim p(t) = \frac{\mathrm{d}}{\mathrm{d}t}\mathrm{en}(t) \tag{6}$$

In Figures 14 and 15, (a) and (b) show the ground accelerations and roof-relative displacements, (c) shows the first story drifts, (d) shows the energy and power input into the structure, (e) shows the amplitude envelope of the roof-relative response and (f) shows the 'instantaneous' system frequency, all versus time. Finally, (g) shows the amplitude of the roof-relative response versus the instantaneous frequency. In (e), the thicker curve shows the amplitude envelope obtained by Gabor transform, and the thinner line—using analytic signal representation [3]. The curves in (f) and (g) are the results of time–frequency analysis using Gabor transform. The numbered open circles appearing in different parts of Figures 14 and 15 indicate different instants of time.

The analysis of novelties indicated that the damage occurred at times about 6.4, 8.2–9.2 and 11.2 s, which agree with the times of large drift amplitudes (c). Based on these times, the decrease of frequency prior to 6.4 s (g) was likely not due to the major damage. A comparison with the time history of power input (d) suggests that the major damage followed large pulses of the input power, within about 2 s. A comparison with the changes in system frequency shows that there was a drop in frequency following the first occurrence of damage. The drop of NS frequency was significant ($\sim$43%) after $t = 6.4$ s when the damage started to occur, while the

DOI: 10.1002/stc

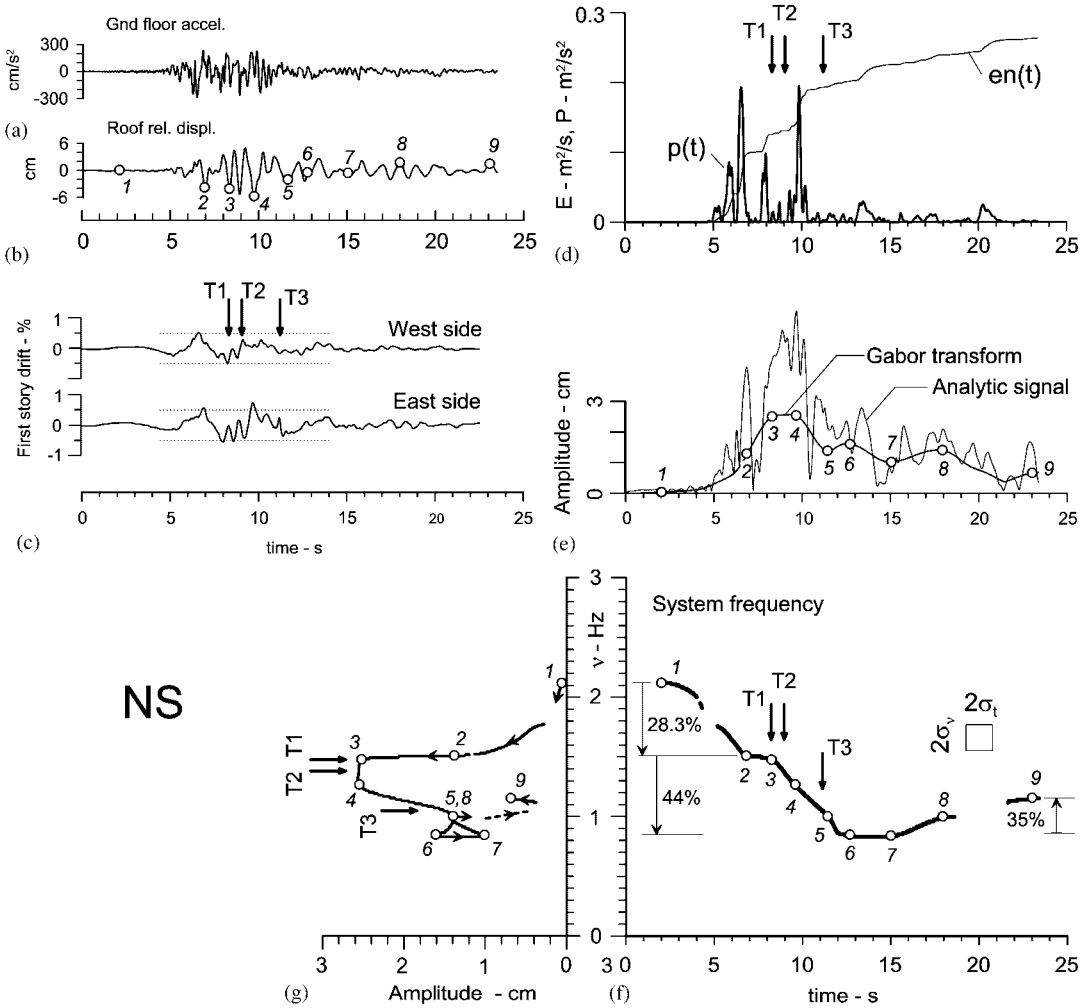

Figure 14. Comparison of results of time–frequency analysis [3], novelty analysis (this paper), drifts [3] and input power for NS motions (this paper).

drop of the EW frequency was smaller ($\sim$21%), especially following the collapse of the first story columns at 11.2 s. The drop in system frequency was in part but not entirely caused by the severe damage (see [31] for example analysis of the degree to which the changes in the system frequency of a nine-story reinforced concrete building can be due to changes in the structure as opposed to changes in the soil and foundation system).

Quality of the data used

The data used in this study were recorded by force balance accelerometers and analog CR-1 film recorder [32,33]. Having dynamic range limited to about 10 bits of digital resolution, these data may seem 'noisy' relative to data recorded by modern analog to digital converters and recorders.

DOI: 10.1002/stc

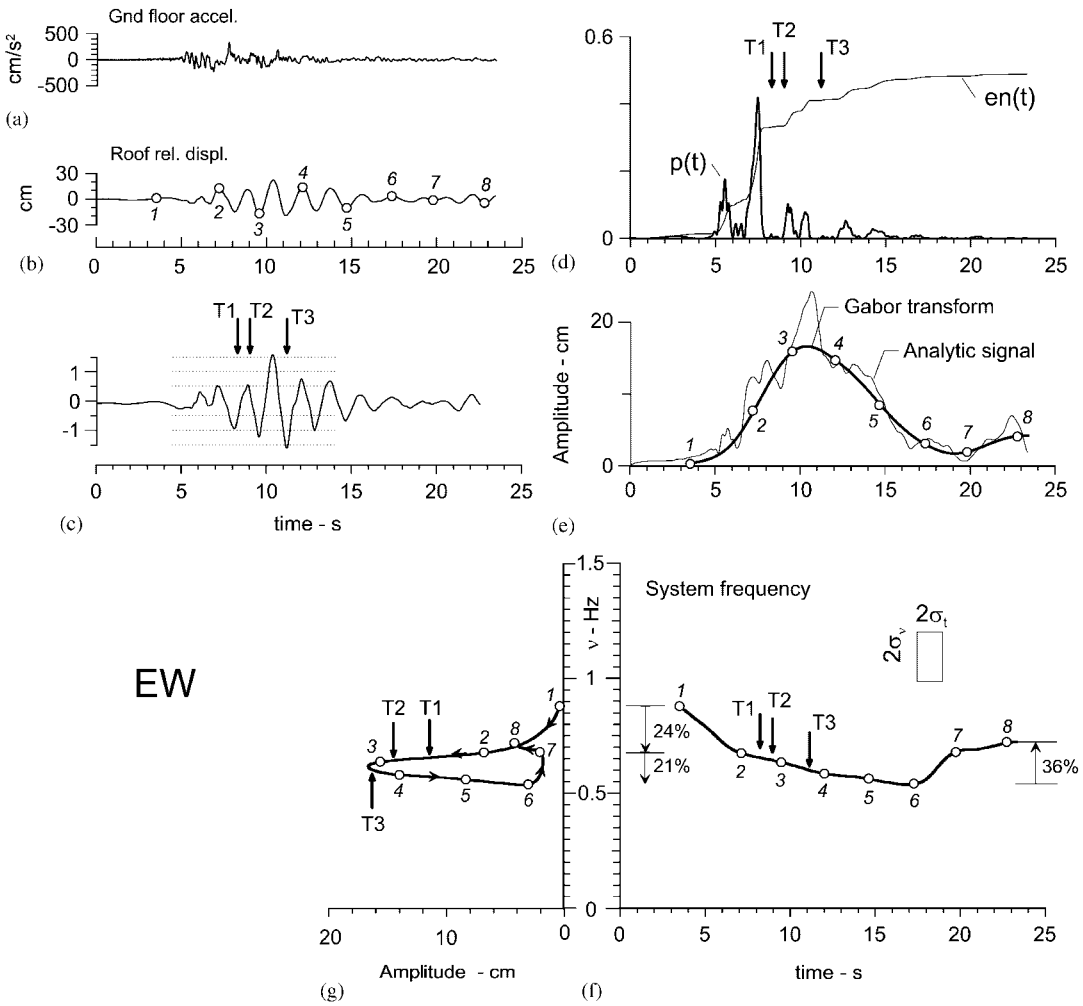

Figure 15. Same as Figure 14 but for EW motions.

We note that, while recorders with higher dynamic range record transducer output with smaller noise amplitudes, they do not necessarily produce more information, unless all six components of motion (three translations and three rotations) have been recorded. This is because point rotations, angular accelerations, cross axis sensitivity and misalignment errors, all neglected in the instrument correction and data processing of digitally recorded data, are above the recording noise, and collectively contribute to 'noise' that is comparable to the noise of the analog recorders [34]. Unless all six components of motion have been recorded simultaneously, and the transducers orientation has been determined accurately by field calibration [35,36], so that complete instrument correction can be performed [33,35–38], there is little advantage in recording tanslational strong motions with resolution much higher than 10–11 bits. The data used in this paper were digitized by the second author using Optronics rotating drum scanner with square pixels of 25 μ [28,39], corresponding to sampling rate of 400 points per second, which is

DOI: 10.1002/stc

comparable to or better than the sampling rate of most digital accelerographs available at the time of this earthquake [32]. For meaningful comparison of the timing of the novelties recorded by different channels, it is important to have all recorded motions corrected to the same origin in time. Our processing method [28] corrects routinely for time shifts caused by different projection angles of the analog traces onto the film, in contrast to all older analog digitization procedures. Based on our long experience with automatic digitization of many accelerogams, we believe that the accuracy of the relative timing of the different traces is about 0.01 s or better.

SUMMARY AND CONCLUSIONS

An analysis of novelties is presented for the NS and EW acceleration responses of the ICS building to the 1979 Imperial Valley earthquake, which severely damaged the building. The objective was to explore the use of novelties for the detection of damage in real structures, and to see what further insight the novelties could provide into the occurrence of damage. The novelties were detected using an expansion of the motion in series of bi-orthogonal wavelets, in particular, as spikes in the distribution of squared coefficients of the sub-band 12.5–25 Hz.

The analysis showed the following: (1) The spatial distribution and relative magnitudes of the detected novelties were generally consistent with the spatial distribution and degree of the observed damage [1]. (2) The time of occurrence of the major damage, suggested by the novelties, agrees with the time of significant drops in the NS and EW system frequencies reported earlier [3], which are estimated based on information contained in the low-frequency part of the spectrum of response (<2 Hz), disjoint form the sub-band in which the novelties are detected (12.5–25 Hz). (3) These times also agree with times of occurrence of large drifts, which are also mostly due to energy in the low-frequency part of the spectrum of the building response. (4) The major damage followed large pulses of input power within about 2 s. (5) The method we presented in this paper was more effective in the analysis of NS response, which was recorded by a spatially denser array (along three vertical lines, at both ends and at the center of the building), than in the analysis of the EW response (recorded only at the center of the floor slabs). (5) The novelties were an order of magnitude larger in the NS response, in which the building was stiffer. (5) The time delays between novelties detected in different channels, but apparently due to a common event, indicate velocities of propagation of the disturbances within the structure consistent with independent estimates from the first NS and EW system frequencies.

It is concluded that this method, applied to data were recorded by analog accelerographs, could identify the time of occurrence and roughly the spatial distribution and degree of the major damage in the ICS building, which in this case was severe. The time resolution of this method is superior to that of the time–frequency analysis, but its spatial resolution, and the ability to detect reliably the degree of damage can be limited by the density of deployed sensors. Yet, even with limited number of sensors, this method can provide useful information and insight into the occurrence of damage.

ACKNOWLEDGEMENTS

The seismic monitoring array in the ICS building was operated by California Geological Survey (formerly California Division of Mines and Geology).

DOI: 10.1002/stc

REFERENCES

1. Kojić S, Trifunac MD, Anderson JC. A post earthquake response analysis of the Imperial County Services Building in El Centro. *Report CE 84-02*, Department of Civil Engineering, University of Southern California, Los Angeles, CA, U.S.A., 1984.
2. Jordanovski LR, Trifunac MD. Least square inversion with time shift optimization and an application to earthquake source mechanism. *Soil Dynamics and Earthquake Engineering* 1990; **9**(5):243–254.
3. Todorovska MI, Trifunac MD. Damage detection in the Imperial County Services Building I: the data and time–frequency analysis. *Soil Dynamics and Earthquake Engineering* 2007; **27**:564–576.
4. Ghobarah A. On drift limits associated with different damage levels. *Proceedings of the International Workshop on Performance-Based Design*, Bled, Slovenia, 28 June–1 July 2004; 321–332.
5. Todorovska MI. Earthquake damage: detection and early warning in man-made structures. In *Encyclopedia of Complexity and System Science*, Meyers RA (ed.), Section on Complexity in Earthquakes, Tsunamis, and Volcanoes, and Forecasting and Early Warning of their Hazards, Lee WHK (Section ed.). Springer: Berlin, 2009.
6. Todorovska MI. Seismic interferometry of a soil–structure interaction model with coupled horizontal and rocking response. *Bulletin of the Seismological Society of America* 2009; **99**(2A):611–625. DOI: 10.1785/0120080191.
7. Todorovska MI, Trifunac MD. Earthquake damage detection in the Imperial County Services Building III: analysis of wave travel times via impulse response functions. *Soil Dynamics and Earthquake Engineering* 2008; **28**(5):387–404.
8. Sone A, Yamamoto S, Nakaoka A, Masuda A. Health monitoring system of structures based on orthonormal wavelet transform. *Proceedings of the ASME Pressure Vessels and Piping Conference*, *PVP*, vol. 312, 1995; 161–167.
9. Wang Q, Deng X. Damage detection with special wavelets. *International Journal of Solids and Structures* 1998; **36**:3443–3468.
10. Vincent HT, Hu S-L, Hou Z. Damage detection using empirical mode decomposition method and a comparison with wavelet analysis. *Proceedings of the 2nd International Workshop on Structural Health Monitoring*, Stanford University, Stanford, CA, U.S.A., 8–10 September 1999.
11. Corbin M, Hera A, Hou Z. Locating damage regions using wavelet approach. *Proceedings of the Fourteenth Engineering Mechanics Conference*, ASCE, Department of Civil Engineering, University of Texas, Austin, TX, U.S.A., 22–24 May 2000.
12. Hou Z, Noori M, Amand R. Wavelet-based approach for structural damage detection. *Journal of Engineering Mechanics* (ASCE) 2000; **126**(7):677–683.
13. Pan T-S, Lee CL. Application of wavelet theory to identify yielding in seismic response of bi-linear structures. *Soil Dynamics and Earthquake Engineering* 2002; **31**:379–398.
14. Hera A, Hou Z. Application of wavelet approach for ASCE structural health monitoring benchmark studies. *Journal of Engineering Mechanics* (ASCE) 2004; **130**(1):96–130.
15. Worden K, Manson G, Allman D. Experimental validation of a structural health monitoring methodology. Part I. Novelty detection on a laboratory structure. *Journal of Sound and Vibration* 2003; **259**(2):323–343.
16. Manson G, Worden K, Allman D. Experimental validation of a structural health monitoring methodology. Part II. Novelty detection on a Gnat aircraft. *Journal of Sound and Vibration* 2003; **259**(2):345–363.
17. Manson G, Worden K, Allman D. Experimental validation of a structural health monitoring methodology. Part III. Damage location on an aircraft wing. *Journal of Sound and Vibration* 2003; **259**(2):365–385.
18. Rezai M, Rahmatian P, Ventura C. Seismic data analysis of a seven-storey building using frequency response function and wavelet transform. *Proceedings of the NEHRP Conference and Workshop on Research on the Northridge*, *California Earthquake of January 17*, *1994*. CURE, Oakland, CA, vol. 1, 1998; 421–428.
19. Todorovska MI, Trifunac MD. Structural health monitoring by detection of abrupt changes in response using wavelets: application to a 6-story RC building damaged by an earthquake. *Proceedings of the 37th Joint Panel Meeting on Wind and Seismic Effects*, Tsukuba, Japan, U.S.–Japan Natural Resources Program (UJNR), 16–21 May 2005; 20.
20. Todorovska MI, Trifunac MD. Damage detection in a 6-story reinforced concrete building using wavelets. *Proceedings of the Earthquake Engineering in the 21st Century* (*EE-21C*), Skopje-Ohrid, Macedonia, 27 August–1 September 2005; 10.
21. Mallat SG. Multiresolution approximations and wavelet orthonormal bases of $L_2(R)$. *Transactions of the American Mathematical Society* 1989; **315**:69–87.
22. Vetterli M, Kovačević J. *Wavelets and Sub-band Coding*. Prentice-Hall PTR, Upper Saddle River, NJ, 1995.
23. Misiti M, Misiti Y, Oppenheim G, Poggi J. *Wavelet Toolbox User's Guide*. The Mathworks Inc., Natick, MA, 2002.
24. Todorovska MI, Hao T-Y. Information granulation and dimensionality reduction of seismic data vibration monitoring data using orthonormal discrete wavelet transform for possible application to data mining. *Report CE 03-02*, Department of Civil Engineering, University of Southern California, Los Angeles, CA, 2003.
25. Gičev V, Trifunac MD. Permanent deformations and strains in a shear building excited by a strong motion pulse. *Soil Dynamics and Earthquake Engineering* 2007; **27**(8):774–792.
26. Gičev V, Trifunac MD. Energy and power of nonlinear waves in a seven story reinforced concrete building. *Indian Society of Earthquake Technology Journal* 2007; **44**(1):305–323.

DOI: 10.1002/stc

27. Gičev V, Trifunac MD. Rotations in a shear beam model of a seven-story building caused by nonlinear waves during earthquake excitation. *Structural Control and Health Monitoring* 2009; DOI: 10.1002/stc.264. Published online in 2008.
28. Lee VW, Trifunac MD. Automatic digitization and processing of accelerograms using PC. *Department of Civil Engineering Report 90-03*, University of Southern California, Los Angeles, CA, 1990.
29. Trifunac MD. Zero baseline correction of strong-motion accelerograms. *Bulletin of the Seismological Society of America* 1971; **61**(5):1201–1211.
30. Trifunac MD, Hao TY, Todorovska MI. On energy flow in earthquake response. *Department of Civil Engineering Report CE 01-03*, University of Southern California, Los Angeles, CA, 2001.
31. Todorovska MI. Soil-structure system identification of Millikan Library North-South response during four earthquakes (1970–2002): what caused the observed wandering of the system frequencies? *Bulletin of the Seismological Society of America* 2009; **99**(2A):626–635. DOI: 10.1785/0120080333.
32. Trifunac MD, Todorovska MI. Evolution of accelerographs, data processing, strong motion arrays and amplitude and spatial resolution in recording strong earthquake motion. *Soil Dynamics and Earthquake Engineering* 2001; **21**(6):537–555.
33. Amini A, Trifunac MD. Analysis of force balance accelerometer. *Soil Dynamics and Earthquake Engineering* 1985; **4**(2):83–90.
34. Trifunac MD, Todorovska MI. A note on the useable dynamic range of accelerographs recording translation. *Soil Dynamics and Earthquake Engineering* 2001; **21**(4):275–286.
35. Todorovska MI. Cross-axis sensitivity of accelerographs with pendulum like Transducers-Mathematical Model and the Inverse Problem. *Earthquake Engineering and Structural Dynamics* 1998; **27**(10):1031–1051.
36. Todorovska MI, Novikova EI, Trifunac MD, Ivanović SS. Advanced accelerograph calibration of the Los Angeles Strong Motion Array. *Earthquake Engineering and Structural Dynamics* 1998; **27**(10):1053–1068.
37. Trifunac MD. A note on correction of strong-motion accelerograms for instrument response. *Bulletin of the Seismological Society of America* 1972; **62**:401–409.
38. Wong HL, Trifunac MD. Effects of cross-axis sensitivity and misalignment on response of mechanical-optical accelerographs. *Bulletin of the Seismological Society of America* 1977; **67**:929–956.
39. Trifunac MD, Lee VW, Todorovska MI. Common problems in automatic digitization of strong motion accelerograms. *Soil Dynamics and Earthquake Engineering* 1999; **18**(7):519–530.